Journal of Hazardous Materials 186 (2011) 1360–1366

Contents lists available at ScienceDirect

Journal of Hazardous Materials

journal homepage: www.elsevier.com/locate/jhazmat

Mn–Ce oxide as a high-capacity adsorbent for fluoride removal from water

Shubo Deng[a,b], Han Liu[a], Wei Zhou[a], Jun Huang[a,b], Gang Yu[a,b,*]

[a] Department of Environmental Science and Engineering, Tsinghua University, Beijing 100084, China
[b] POPs Research Center, Tsinghua University, Beijing 100084, China

ARTICLE INFO

Article history:
Received 9 September 2010
Received in revised form 3 December 2010
Accepted 6 December 2010
Available online 14 December 2010

Keywords:
Defluoridation
Fluoride
Mn–Ce oxide adsorbent
Adsorption capacity
Adsorption mechanism

ABSTRACT

A novel Mn–Ce oxide adsorbent with high sorption capacity for fluoride was prepared via co-precipitation method in this study, and the granular adsorbent was successfully prepared by calcining the mixture of the Mn–Ce powder and pseudo-boehmite. High-resolution transmission electron microscopy (TEM) image showed that the Mn–Ce adsorbent consisted of about 4.5 nm crystals, and X-ray diffraction (XRD) analysis indicated the formation of solid solution by Mn species entering CeO_2 lattices. The surface hydroxyl group density on the Mn–Ce adsorbent was determined to be as high as 15.3 mmol g^{-1}, mainly responsible for its high sorption capacity for fluoride. Sorption isotherms showed that the sorption capacities of fluoride on the powdered and granular adsorbent were 79.5 and 45.5 mg g^{-1} respectively at the equilibrium fluoride concentration of 1 mg L^{-1}, much higher than all reported adsorbents. Additionally, the adsorption was fast within the initial 1 h. Fourier transform infrared (FTIR) and X-ray photoelectron spectroscopy (XPS) analysis revealed that the hydroxyl groups on the adsorbent surface were involved in the sorption of fluoride. Both anion exchange and electrostatic interaction were involved in the sorption of fluoride on the Mn–Ce oxide adsorbent.

1. Introduction

Fluoride contamination in groundwater is a worldwide problem, and its concentration in drinking water of many places exceeds the permissible values [1]. The maximal fluoride concentration of 1.5 mg L^{-1} has been recommended in drinking water by World Health Organization [2], while the standard of fluoride concentration in drinking water is 1.0 mg L^{-1} in China. Adsorption is one of the most important methods for water defluoridation, especially for individual homes in rural areas. Many adsorbents such as activated alumina, bone char, layered double hydroxides, clay, and fly ash have been used for fluoride removal [3–6]. Among them, activated alumina is the most commonly used adsorbent for water defluoridation, but its disadvantages including aluminum dissolution and relatively low sorption capacity prevent it from wide application. Although bone char normally has higher sorption capacity for fluoride than activated alumina, its application is limited since it is derived from animal bone and unacceptable for some residents on religious grounds among various communities. Some natural adsorbents such as minerals and clay are cost-effective, but their sorption capacities for fluoride are not high enough for actual application [1,7], and thus much effort has been devoted to develop new efficient adsorbents in recent years.

To increase the sorption capacity of fluoride, La, Ce, and Zr are usually doped in some metal oxides or loaded in porous materials to prepare the efficient adsorbents. The hybrid adsorbents including Fe–Zr oxides, Fe–Al–Ce trimetal oxides, La-modified chitosan, Zr-impregnated collagen fiber, Ce–Al oxides, as well as La and Zr-loaded zeolite have been reported to have high sorption capacity for fluoride [8–13]. The enhanced sorption capacities are attributed to the high affinity of these special elements to fluoride, but the substantial mechanism is not fully elucidated. Evidently, doping La, Ce, and Zr in other metal oxides is an efficient method to prepare some novel adsorbents with high sorption capacity for fluoride.

Although many inorganic adsorbents have been prepared and used to remove fluoride in the literature, they are normally in the powder form. In actual water treatment, the granular adsorbents are required to pack in a column to remove fluoride from water. Calcination is often used to granulate some powders, but it cannot be applied to many inorganic adsorbents used for fluoride removal due to the significant lose of sorption capacity. Other granulation methods such as the addition of polyvinyl acetate are also not very satisfactory in terms of sorption capacity and mechanical strength [14,15]. How to prepare the granular adsorbent with high sorption capacity for fluoride is crucial for actual water defluoridation.

In this study, the novel Mn–Ce hybrid oxide adsorbent with high sorption capacity for fluoride was prepared through the co-

* Corresponding author at: Department of Environmental Science and Engineering, Tsinghua University, Beijing 100084, China. Tel.: +86 10 62787137; fax: +86 10 62794006.
E-mail addresses: dengshubo@tsinghua.edu.cn (S. Deng), yg-den@tsinghua.edu.cn (G. Yu).

0304-3894/$ – see front matter © 2010 Elsevier B.V. All rights reserved.
doi:10.1016/j.jhazmat.2010.12.024

precipitation method, and especially the granular adsorbent with little lose of sorption capacity was successfully prepared via calcining the mixture of pseudo-boehmite and adsorbent powder. The optimal adsorbent was characterized by TEM, XRD, and surface hydroxyl group analysis. The batch experiments including sorption kinetics and isotherms were studied in detail, and the possible sorption mechanism was also elucidated by the FTIR and XPS analysis.

2. Materials and methods

2.1. Materials

$Ce(NO_3)_3{\cdot}6H_2O$ and $MnSO_4{\cdot}H_2O$ were purchased from Sinopharm Chemical Reagent Co., Ltd. (China) and were of reagent grade. Pseudo-boehmite was provided by Shandong Branch Company, Aluminum Corporation of China Limited. 1000 mg L^{-1} fluoride stock solution was prepared by dissolving NaF in 1 L of deionized water from a Milli-Q water system.

2.2. Powdered adsorbent preparation

A certain amount of $Ce(NO_3)_3{\cdot}6H_2O$ was added to 0.2 mol L^{-1} $MnSO_4$ solution to prepare solution at a predetermined Ce/Mn ratio. Solution pH was adjusted to 7.4–7.8 by dropwise adding 4 mol L^{-1} NaOH under vigorous stirring. The precipitate was obtained by filtration and rinsed with deionized water, followed by a drying process at 80–600 °C for 6 h. Finally, the dried adsorbent was ground into fine powder below 200 mesh.

2.3. Adsorbent granulation

The Mn–Ce adsorbent powder and pseudo-boehmite powder were mixed at a mass ratio of 3/1 and homogenized by stirring with a glass rod. Thereafter, 0.5 mol L^{-1} HNO_3 was added to the mixture, and the mass of HNO_3 added equaled to 20% mass of pseudo-boehmite powder. Deionized water which weight equaled to 40% weight of dry powder was then added, and the mixture was homogenized by stirring. The product was squeezed to favorable shapes and dried at 80 °C for 12 h. After that, the dried product was calcined in a Muffle furnace at 400 °C for 40 min. The obtained granular adsorbent was sieved, and those granules in the size range of 0.3–1.0 mm were used for adsorption experiments.

2.4. XRD analysis

X-ray diffraction analysis was carried out in D/max-IIIV powder diffractometer using Cu Kα radiation at a scanning range of $2\theta = 10–80°$ with a speed of 6° min^{-1} and a scan step of 0.02°. The adsorbent samples including the Mn–Ce hybrid oxide, manganese oxide, and cerium oxide dried at 80 °C were analyzed.

2.5. FTIR spectroscopy

The Mn–Ce adsorbent calcined at 400 and 800 °C, as well as the adsorbent after fluoride sorption at 10, 50 and 100 mg L^{-1}, were blended with KBr, and then pressed into disks for FTIR analysis. Scans were repeated 32 times in the wavenumber range of 400–4000 cm^{-1}, and the spectra were recorded on a FTIR spectrophotometer (Nicolet 6700, USA) under ambient conditions.

2.6. TEM analysis

The Mn–Ce adsorbent powder was observed using a high resolution TEM (JEOL 2011, Japan), operated at an accelerating voltage of 200 kV. The sample was placed into ethanol and dispersed by ultrasonic, and then some droplets taken from the supernatant were placed on a copper net and dried under ambient conditions before observation.

2.7. Determination of hydroxyl group density

The amount of surface hydroxyl groups on oxide samples was measured by the titration method described in the literature [16]. Briefly, 0.3 g of oxide was added into 50 mL of 20–90 mM NaOH solution. After the mixture was shaken at 25 °C for 4 h, the solution was passed through a 0.22 μm cellulose membrane, and HCl was used to neutralize the residual NaOH in filtrate. The amount of hydroxyl group on the oxide can be calculated according to the amount of NaOH consumed.

2.8. XPS analysis

The Mn–Ce adsorbent before and after fluoride sorption was analyzed using XPS (PHI Quantera 5300X, Japan) with an Al Kα X-ray source (1486.71 eV of photons) to determine the C, O, Ce, and Mn contents on the adsorbent surface. The operation condition and data analysis were described in our previous paper [17].

2.9. Sorption experiments

Batch sorption experiments were conducted to examine the adsorption isotherm and kinetics of fluoride. The sorption experiments were carried out in 250 mL polypropylene flasks containing 100 mL of fluoride solution and 0.01 g adsorbent, and the flasks were shaken at 150 rpm in a shaker at 25 °C for 24 h. In the sorption isotherm experiment, fluoride solution at different concentrations was prepared, and solution pH was adjusted to 6, 7 or 8, and kept relatively constant in the error range of ±0.2 throughout the sorption experiment by adding NaOH or HCl solution. The adsorption kinetic experiment was carried out at the initial fluoride concentration of 10 mg L^{-1}, and the solution pH value was 6. After the sorption experiments, the adsorbent was separated from the solution by a filter with a 0.22 μm cellulose membrane, and the residual fluoride concentration in solution was measured by a fluoride meter equipped with fluoride ion selective electrode (Thermo Orion, USA).

3. Results and discussion

3.1. Adsorbent preparation

In the adsorbent preparation, the Ce/Mn molar ratio and drying temperature had significant effect on the sorption capacity of fluoride. As shown in Fig. 1a, the sorption capacities of fluoride on the Mn–Ce oxide adsorbent dried at 80 °C first increased and then decreased with the increase of Ce/Mn molar ratios from 2/1 to 1/50. The highest sorption capacity of 85.1 mg g^{-1} was achieved at the Ce/Mn molar ratio of 1/1, which was much higher than 36.9 mg g^{-1} on the cerium oxide and 2.8 mg g^{-1} on the manganese oxide. This result verified the synergistic effect of Mn and Ce compounds in the preparation. The specific surface areas of powdered cerium oxide, manganese oxide, and Mn–Ce hybrid oxides were measured to be 136, 23, and 41 m^2 g^{-1}, respectively, indicating that the specific surface area was not the main reason for the high sorption capacity of fluoride on the powered Mn–Ce oxide adsorbent. In Fig. 1a, it can be seen that the adsorbent prepared at the Ce/Mn molar ratio of 1/2 had the sorption capacity very close to the highest value, and especially less cerium was used in the preparation. Therefore, the Ce/Mn molar ratio of 1/2 was used in the following preparation and sorption experiments.

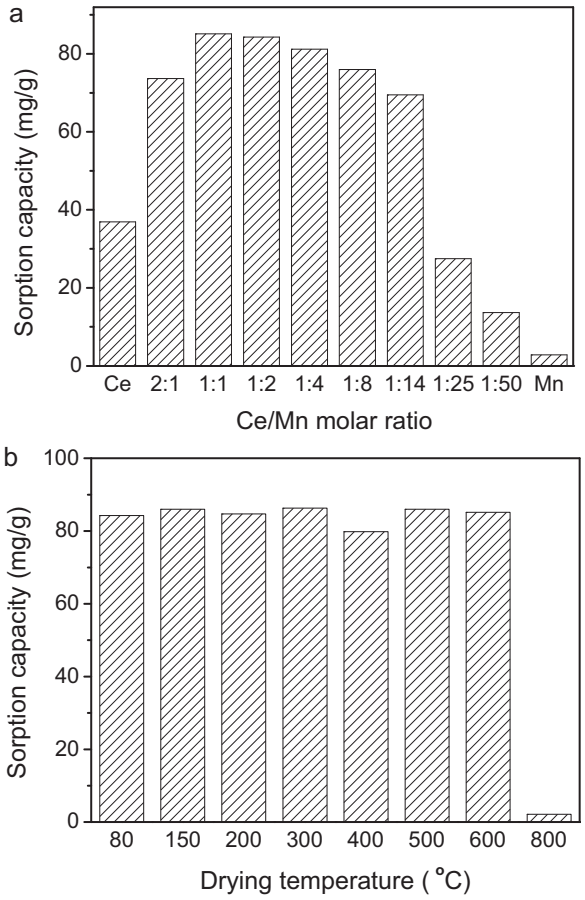

Fig. 1. Effect of (a) Ce/Mn molar ratio and (b) drying temperature on the sorption capacity of fluoride on the powdered Mn–Ce oxide adsorbent with 0.01 g adsorbent in 100 mL of 10 mg L^{-1} fluoride solution at pH 6 for 24 h.

Fig. 1b illustrates the effect of drying temperature on the sorption capacity of fluoride on the Mn–Ce adsorbent. The sorption capacity was almost constant when the drying temperature increased from 80 °C to 600 °C, but it significantly decreased to 2.1 mg g^{-1} when the adsorbent was calcined at 800 °C. The calcination at high temperature might destroy the adsorbent structure and decrease the surface hydroxyl group, resulting in the low sorption capacity [12]. Since the Mn–Ce hybrid adsorbent had high thermal stability up to 600 °C, it can be granulated by the calcination.

In actual water treatment, granular adsorbents are usually required to remove fluoride from water. Although many methods can be used to granulate powdered adsorbents, their sorption capacities often decrease significantly after granulation. By now, no satisfactory granulation method can be applied to prepare granular adsorbents for fluoride removal. In our study, we found that the novel granular Mn–Ce adsorbent was successfully prepared by mixing the adsorbent powder with pseudo-boehmite powder and calcining at 400 °C, which was described in the section of adsorbent granulation. This granulation procedure was similar to the preparation of porous activated alumina, and activated alumina acted as a porous carrier for the Mn–Ce adsorbent. The pseudo-boehmite and Mn–Ce powders were mixed with a little water in the granulation, and thus the pseudo-boehmite (AlOOH) changed to activated alumina (Al_2O_3) after the calcination at 400 °C. When the granular adsorbent was used to adsorb fluoride under the same conditions, the sorption capacity was up to 72 mg g^{-1}, a little lower than that of the powdered adsorbent. Since activated alumina had low sorption capacity for fluoride, the loaded Mn–Ce oxide in the porous particles was responsible for the high sorption capacity. The granular Mn–Ce adsorbent had large specific surface area (25.3 m^2 g^{-1}) and strong mechanical strength. When the granular adsorbent was place into water, its strength did not decrease. Evidently, the granular adsorbent prepared by this novel method had a promising application in water treatment for fluoride removal.

3.2. Adsorbent characterization

The TEM image of the Mn–Ce adsorbent prepared at the Ce/Mn molar ratio of 1/2 is shown in Fig. 2. The adsorbent is well crystallized with clear lattice stripes, and the nanocrystalline grain of the hybrid adsorbent was highlighted in the elliptic region and its diameter was about 4.5 nm. The aggregates of nanocrystalline grains formed in the preparation, and their sizes ranged from around 20 nm to several microns. The inset on the up right image gave a closer view of lattice stripes of a single crystal grain whose interplanar distance was estimated to be 0.30 nm, very close to 0.32 nm for (1 1 1) facet of pure CeO_2 [18]. The presence of CeO_2 in the hybrid adsorbent was verified by XRD analysis in the following section. The (1 1 1) facet interplanar distance of the hybrid adsorbent was smaller than that of pure CeO_2. This may be attributed to the partial replacement of larger Ce species with smaller Mn species in CeO_2 lattices and the formation of solid solution, which will be further discussed in the following XRD analysis.

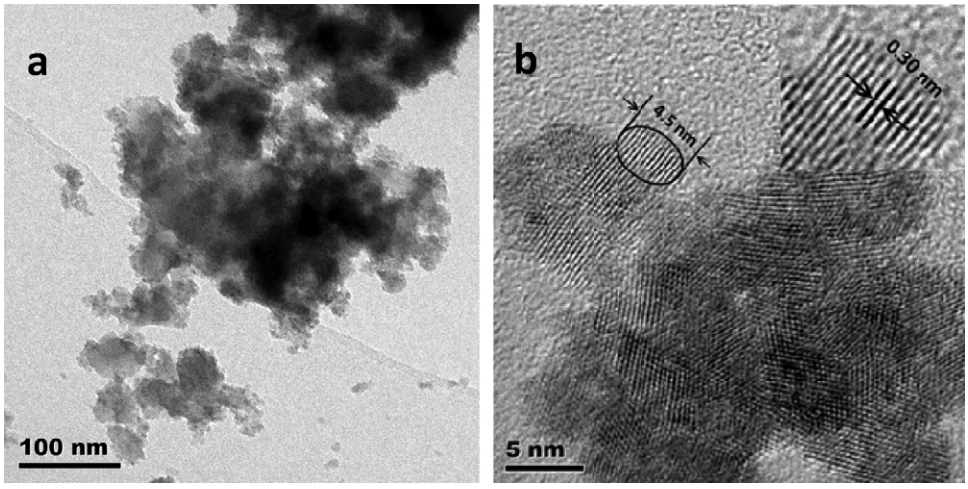

Fig. 2. TEM image of the powdered Mn–Ce oxide adsorbent prepared at Ce/Mn molar ratio of 1/2.

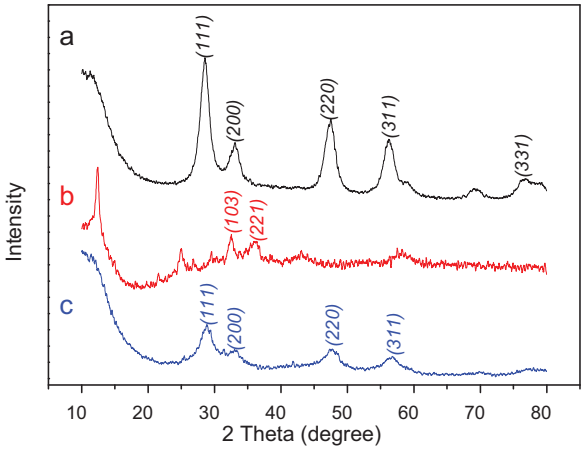

Fig. 3. XRD patterns of the (a) cerium oxide, (b) manganese oxide, and (c) powdered Mn–Ce adsorbent prepared at Ce/Mn molar ratio of 1/2.

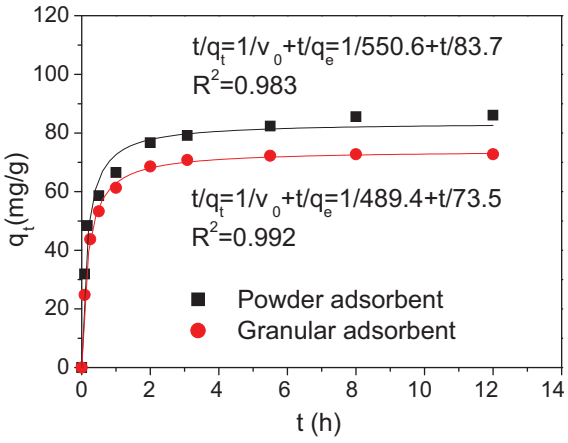

Fig. 4. Sorption kinetics of fluoride on the powdered and granular Mn–Ce oxide adsorbent and modeling result using the pseudo-second-order model.

Fig. 3 illustrates the XRD patterns of the Mn–Ce adsorbent as well as manganese and cerium oxides. The diffraction peaks in Fig. 3a were found at 28.55°, 33.08°, 47.49° and 56.35°, which were the characteristic peaks of CeO_2 [12]. The manganese oxide exhibited the major peaks at 32.52° and 36.15°, indicating that Mn_3O_4 was the dominant species [19]. The XRD pattern of Mn–Ce adsorbent is shown in Fig. 3c, and the dominant characteristic diffraction peaks indicated the presence of crystalline CeO_2 [12]. Manganese oxide phase was hardly detected in the XRD pattern because of either little presence of manganese oxide in the adsorbent or the formation of Mn–Ce solid solution in which case the Mn species entered the lattices of CeO_2. Interestingly, the major diffraction peaks of Mn–Ce adsorbent were at 28.87°, 33.33°, 47.81° and 56.84°, all showing a progressive shift of diffraction peaks to higher Bragg angles compared to the pure CeO_2. This shift can be explained by the contraction of unit cell after Mn species entering the lattices of CeO_2 and forming the Mn–Ce solid solution, since the radius of Mn ion was smaller than that of Ce ion (Mn^{2+} = 0.083 nm, Mn^{3+} = 0.0645 nm, Ce^{4+} = 0.097 nm) [20]. The contraction of unit cell also led to the decrease of (1 1 1) facet interplanar distance of Mn–Ce hybrid adsorbent, which was observed by TEM. Therefore, this result further verified the formation of Mn–Ce solid solution, and the hybrid adsorbent was more than simple mixture of two kinds of oxides. Furthermore, the diffraction peak broadening was observed in the Mn–Ce hybrid adsorbent, indicating more defective CeO_2 lattices and lower crystallinity.

Surface hydroxyl group density is one critical factor in explaining high sorption capacity of fluoride on the adsorbents since hydroxyl group is usually responsible for fluoride sorption through anion exchange [17]. The density of surface hydroxyl group on the manganese oxide, cerium oxide, powdered and granular Mn–Ce adsorbent was determined to be 5.9, 2.2, 15.3 and 11.7 mmol g^{-1}, respectively. Evidently, the powdered and granular Mn–Ce hybrid adsorbent exhibited much higher surface hydroxyl group than manganese oxide and cerium oxide, which was consistent with their sorption capacities for fluoride. Additionally, the density of surface hydroxyl group on the Mn–Ce adsorbent prepared at the Ce/Mn molar ratio of 1/1 and 1/8 was 15.1 and 12.2 mmol g^{-1}, respectively, further indicating that the high sorption capacities of fluoride (see Fig. 1a) were related to the high density of hydroxyl group on the hybrid adsorbent.

Another important factor responsible for the high sorption capacity of Mn–Ce adsorbent involves the creation of activated hydroxyl groups due to the defects of lattices in the hybrid adsorbent. According to the XPS and XRD results, Mn(II), Mn(III) and Ce(III) species existed in the hybrid adsorbent besides the dominant Ce(IV) species, and they entered the lattices of CeO_2 to form solid solution. The lower valent ionic substitution created oxide ion vacancy to balance the charges, thus forming the distorted oxygen sublattices. The distorted oxygen sublattices consisted of shorter and longer Ce(Mn)–O bonds [21]. Therefore, the longer Ce(Mn)–O bonds created by lower valent ionic substitution led to activated lattice oxygen which later would become activated hydroxyl group when the hybrid adsorbent was exposed to aqueous solution. These activated hydroxyl groups were supposed to be easy to exchange with fluoride, increasing the sorption capacity of fluoride on the Mn–Ce adsorbent.

3.3. Sorption kinetics and isotherm

Fig. 4 depicts the sorption kinetics of fluoride on powdered and granular Mn–Ce oxide adsorbent in 10 mg L^{-1} fluoride solution. It can be found that most of the sorption took place in the first 1 h, and then the sorption capacity increased gradually till the equilibrium was reached. It is interesting that the granular adsorbent required 3 h to reach the equilibrium, while the sorption equilibrium was achieved after 8 h for the powdered adsorbent. To further understand the sorption kinetics, the pseudo-second-order model was selected to fit the sorption kinetic data [22]. As shown in Fig. 4, the adsorption of fluoride on the Mn–Ce oxide adsorbent was fitted well by this model, and the equilibrium adsorption capacities (q_e) were 83.7 and 73.5 mg g^{-1} on the powdered and granular adsorbent, respectively. The initial sorption rate (υ_0) was 550.6 mg g^{-1} h^{-1} for the powdered adsorbent, and 489.4 mg g^{-1} h^{-1} for the granular adsorbent. Evidently, the granular Mn–Ce adsorbent still had fast sorption for fluoride, and the granulation had little effect on the sorption kinetics, indicating that fluoride can easily access and diffuse in the granular Mn–Ce adsorbent.

The sorption isotherms of fluoride on the powdered and granular Mn–Ce adsorbents are shown in Fig. 5. The powdered adsorbent had higher sorption capacity than the granular one. Their sorption capacities increased with increasing fluoride concentrations, and maximum value was achieved at the equilibrium fluoride concentration above 6 mg L^{-1} for the powdered adsorbent, and 9 mg L^{-1} for the granular one. To obtain the maximum sorption capacity, the Langmuir equation was used to model the sorption data, and it can be found that this model described the isotherms well according to the correlation coefficient (see Fig. 5). The maximum sorption capacities of fluoride on the powdered and granular Mn–Ce adsorbent were 137.5 and 103.1 mg g^{-1}, respectively. Since the final fluoride concentration must be below the standard value in actual water treatment, the sorption capacity at low fluoride

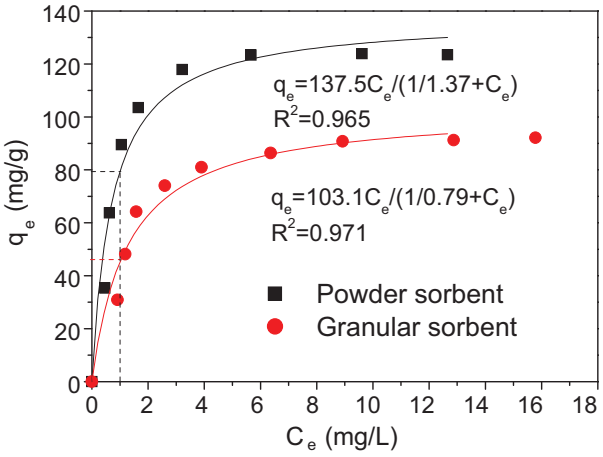

Fig. 5. Sorption isotherms of fluoride on the powdered and granular Mn–Ce oxide adsorbent at pH 6 and modeling using the Langmuir equation ($q_e = q_m C_e/(1/b + C_e)$).

concentration is extremely important. As shown in Fig. 5, the sorption capacity of fluoride on the powdered adsorbent was 79.5 mg g^{-1}, while the granular adsorbent had the sorption capacity of 45.5 mg g^{-1} at the equilibrium fluoride concentration of 1 mg L^{-1}. Table 1 lists some adsorbents with high sorption capacities for fluoride reported in the literature. It can be seen that the synthetic hybrid oxides, especially the Ce and Zr modified adsorbents significantly enhanced the sorption capacity. When the equilibrium fluoride concentration was 1 mg L^{-1}, the sorption capacities on the Fe–Al (hydr)oxide (20.1 mg g^{-1}), Ce–Al oxide (27.5 mg g^{-1}), Fe–Al–Ce trimetal oxide (12.2 mg g^{-1}), and Zr-loaded collagen fiber (14.5 mg g^{-1}) were higher than the conventional activated alumina and bone char [13]. It is obvious that the Mn–Ce oxide adsorbent had the highest sorption capacity for fluoride among the reported adsorbents.

Solution pH had a significant effect on the sorption isotherm of fluoride on the Mn–Ce adsorbent. As illustrated in Fig. S1 (Supplementary Information), the sorption capacities of fluoride at pH 7 and pH 8 on the adsorbent decreased to some extent compared to that obtained at pH 6. The sorption capacities at the equilibrium fluoride concentration of 1 mg L^{-1} were also decreased to 48.4 mg g^{-1} at pH 7 and 14.8 mg g^{-1} at pH 8. In the sorption of fluoride at pH 6, it was found that solution pH increased with increasing sorption time, especially at the early sorption stage, and acid must be added to control the pH value, implying that some hydroxyl groups were exchanged with fluoride and released into solution.

The decrease of sorption capacity with increasing pH indicated that the spent adsorbent might be regenerated in alkaline solution. When the spent Mn–Ce adsorbent obtained in Fig. 4 was placed into 50 mL of 0.5 M NaOH solution for 4 h, the regeneration rate was found to be 92%, indicating that this adsorbent can be regenerated and reused for fluoride removal. In addition, the Mn–Ce adsorbent still had high sorption capacity for fluoride in the presence of SO_4^{2-}, SiO_3^{2-}, HCO_3^-, NO_3^-, and Cl^- (Supplementary Information Fig. S2). Hydrogen phosphate caused the greatest decrease in fluoride sorption, while bicarbonate had the moderate effect.

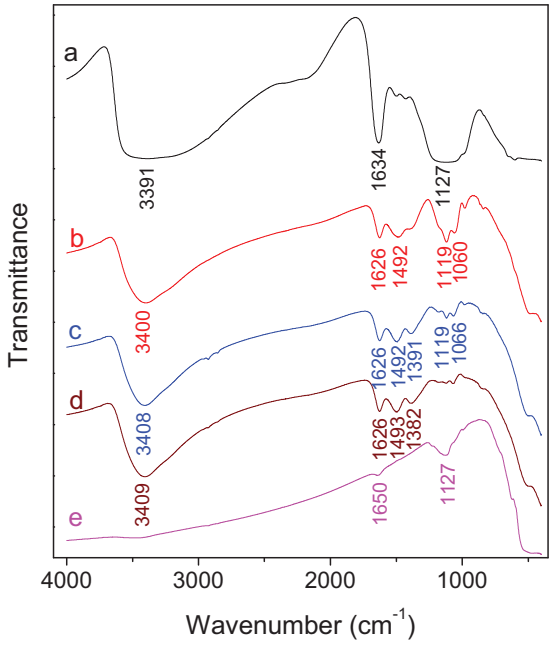

Fig. 6. FTIR spectra of the powdered Mn–Ce oxide adsorbent prepared at Ce/Mn molar ratio of 1/2 (a) before adsorption and after fluoride sorption at (b) 10 mg L^{-1}, (c) 50 mg L^{-1}, and (d) 100 mg L^{-1}, as well as (e) the Mn–Ce adsorbent calcined at 800 °C.

3.4. Sorption mechanism

The FTIR spectra of the Mn–Ce adsorbent after the adsorption of fluoride at different concentrations are depicted in Fig. 6. For the pristine adsorbent, the broad band at 3391 cm^{-1} and the peak at 1634 cm^{-1} could be assigned to the stretching and bending vibration of adsorbed water, and the peak at 1127 cm^{-1} could be attributed to the bending vibration of hydroxyl group on metal oxides [17,30]. After the sorption of fluoride at 10 mg L^{-1}, the bands at 3391 and 1634 cm^{-1} were shifted to 3400 and 1626 cm^{-1}, respectively. Also, the intensity of peak at 1127 cm^{-1} decreased and diverged to two separate peaks at 1119 and 1060 cm^{-1}, which were still assigned for bending vibration of hydroxyl group of metal oxides [30]. It was clearly observed that the intensity of peaks at 1119 and 1060 cm^{-1} continued to decrease with increas-

Table 1
Comparison of sorption capacity of fluoride on some efficient adsorbents.

Adsorbents	Particle size (mm)	Equilibrium con. (mg L^{-1})	Solution pH	Sorption capacity (mg g^{-1})[a]	Ref.
Mesoporous alumina	Powder	50	6.0	7.5	[23]
Mg–Al–CO_3 hydroxides	Powder	1	–	9.74	[24]
MnO_2-coated alumina	0.45–0.90	1	5.2	5.96	[25]
Fe–Al mixed oxides	0.14–0.29	1.5	6.9	12	[26]
Fe–Al–Cr oxides	0.14–0.29	1	5.6	9.29	[27]
Fe_3O_4@$Al(OH)_3$	Powder	1	6.5	20.1	[28]
Fe_2O_3·Al_2O_3·xH_2O	0.5–1.0	1	4	~30	[29]
Fe–Al–Ce oxides	Powder	1	7.0	12.2	[12]
Al–Ce oxides	Powder	1	6	27.5	[13]
Zr-loaded collagen fiber	0.1–0.25	1	5–8	14.5	[10]

[a] Calculated from the sorption isotherms or Langmuir equation.

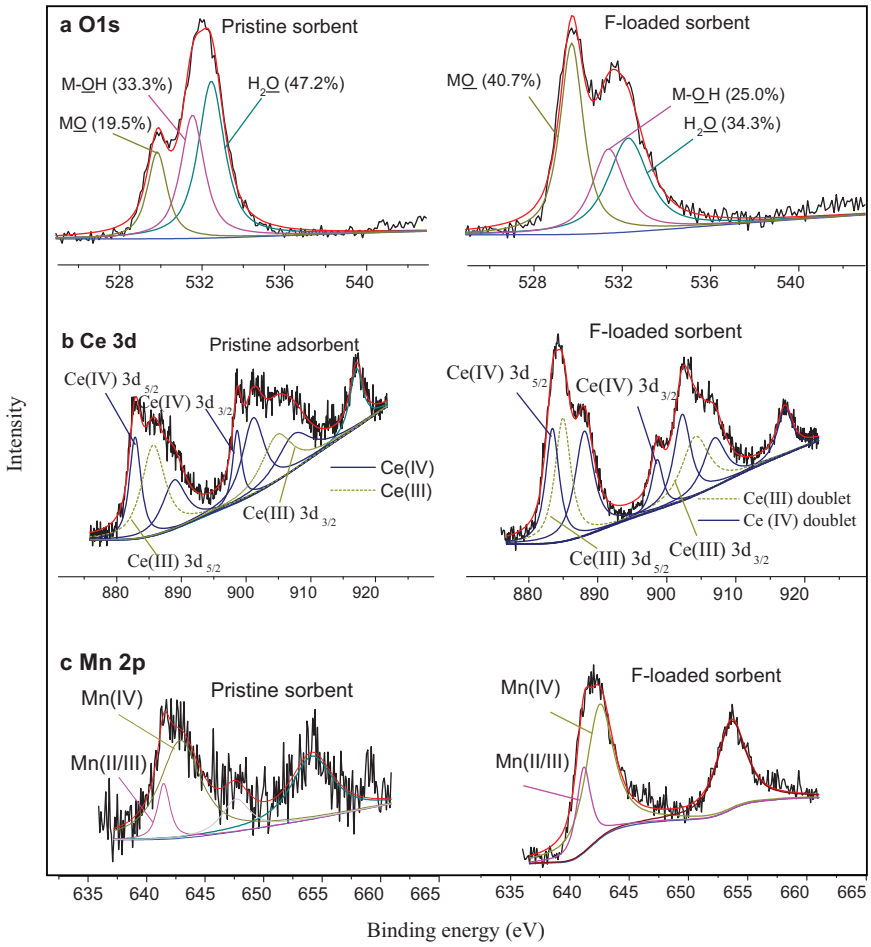

Fig. 7. XPS (a) O 1s (b) Ce 3d (c) Mn 2p core level spectra on the powdered Mn–Ce adsorbent prepared at Ce/Mn molar ratio of 1/2 before and after fluoride sorption.

ing fluoride concentration, and they almost disappeared when the fluoride concentration was 100 mg L^{-1}. Therefore, the surface hydroxyl groups on the hybrid adsorbent were involved in the adsorption of fluoride. It should be pointed out that the broad band at about 3391 cm^{-1} was attributed to the stretching vibration of both the hydroxyl group on metal oxides and adsorbed water, and thus the peak did not disappear after fluoride sorption, but its shape changed. When the adsorbent was calcined at 800 °C, the spectrum exhibited no band at around 3400 cm^{-1} and very low intensity of the peaks at 1650 and 1127 cm^{-1}. This finding indicated that the surface hydroxyl groups on the adsorbent almost disappeared at high calcination temperature, leading to the low sorption capacity for fluoride in Fig. 1b. This result further verified the involvement of surface hydroxyl group in the sorption of fluoride.

To further explore the sorption mechanism of fluoride on the Mn–Ce adsorbent, the adsorbent before and after fluoride adsorption was used for XPS analysis. Fig. 7 shows their O 1s, Ce 3d, Mn 2p XPS spectra. For the pristine adsorbent, the O 1s spectrum was divided into three peaks at 529.8, 531.5, and 532.4 eV, which can be assigned to metal oxide (M–O), hydroxyl bonded to metal (M–OH) and adsorbed water in the adsorbent (H_2O), respectively [17,31,32]. After fluoride adsorption, the area ratio for the peak at 531.5 eV attributed to M–OH decreased from 33.3% to 25.0%, and the area ratio of H_2O also decreased from 47.2% to 34.3%, while the area ratio of M–O increased from 19.5% to 40.7%. The decrease of area ratio at 531.5 eV suggested that hydroxyl groups on the adsorbent surface surely participated in fluoride sorption, which was consistent with result of FTIR analysis.

Fig. 7b illustrates the Ce 3d spectra of the adsorbent before and after fluoride adsorption. Each Ce 3d spectrum was composed of two groups of spin-orbit doublets. The specific peak at 917 eV, arising from a transition from the 4f initial state to the 4f final state, was frequently considered as a confirmation of the presence of Ce(IV) [29]. Both Ce(III) and Ce(IV) were found to exist in the adsorbent. In the spectrum of pristine adsorbent, the peaks at 882.9, 888.9, 898.6, 901.1, and 907.4 eV were considered to belong to Ce(IV). Among them, the peaks at 882.9 and 898.6 eV were attributed to Ce(IV) $3d_{5/2}$ and Ce(IV) $3d_{3/2}$, respectively [30]. The peaks at 885.6 and 904.8 eV were attributed to Ce(III) $3d_{5/2}$ and Ce(III) $3d_{3/2}$, respectively [32,33]. In addition, the molar ratio of Ce(III)/Ce(IV) on the adsorbent was determined to be 1/1.7. After fluoride adsorption, the binding energies at 885.6 and 904.8 eV were decreased to 884.9 and 904.1 eV, respectively. Meanwhile, the peak at 882.9 eV was increased to 883.4 eV. Therefore, the peak shift revealed the possibility that the hydroxyl groups bonded to Ce(III) and Ce(IV) participated in the sorption of fluoride.

The Mn 2p spectra of the adsorbent before and after fluoride sorption are shown in Fig. 7c. Since the binding energies of Mn(II) and Mn(III) were too close to enable a distinct identification, the peak at 641.5 eV was considered to be Mn(II) or Mn(III), and the binding energy at 642.9 eV was attributed to Mn(IV) in the spectrum of Mn–Ce adsorbent [34]. This result indicated that Mn(II) (or Mn(III)) and Mn(IV) were present in the adsorbent, and their ratio was 1/5.8. A decrease of 0.4 eV both for the binding energies of Mn(II) or Mn(III) and Mn(IV) was observed after fluoride adsorption during which their binding energies moved to 641.1 and 642.5 eV, respectively, indicating the hydroxyl groups bonded to Mn species

were also involved in the adsorption of fluoride. Fluoride was possibly adsorbed on the Mn–Ce hybrid adsorbent via the ion-exchange mechanism, which was also verified by other studies [12,13].

Actually, the sorption mechanism of fluoride on the adsorbent is complicated. Since the zero point of surface charge on the adsorbent is at pH 6.5 (Supplementary Information Fig. S3), some hydroxyl groups are protonated at pH 6, and they may adsorb anionic fluoride through electrostatic attraction. At the same time, some unprotonated hydroxyl groups can still exchange with fluoride, resulting in the release of OH^- and increase of solution pH. At higher pH beyond the isoelectric point where surface is negatively charged, only anion exchange between fluoride and hydroxyl groups is involved in the sorption, and thus the sorption capacity decreases. The activated hydroxyl groups formed due to the defects of lattices in the hybrid adsorbent may be easy to contact and exchange with fluoride, leading to the high sorption capacity.

4. Conclusions

A novel Mn–Ce oxide adsorbent with high sorption capacity for fluoride was successfully prepared via co-precipitation method. Sorption isotherms showed that the maximum sorption capacities of fluoride on the powdered and granular Mn–Ce adsorbent were 137.5 and 103.1 mg g^{-1}, respectively, according to the Langmuir fitting. At the equilibrium fluoride concentration of 1 mg L^{-1}, the sorption capacity was 79.5 mg g^{-1} for the powdered adsorbent, and 45.5 mg g^{-1} for the granular one, much higher that all adsorbents reported in the literature. The sorption of fluoride on the granular adsorbent was very fast within the first 1 h, and the sorption equilibrium was achieved after 3 h. The high sorption capacity of fluoride was related to the high density of hydroxyl groups (15.3 mmol g^{-1}) on the Mn–Ce hybrid adsorbent, which was caused by Mn species entering CeO_2 lattices and the creation of activated hydroxyl groups. FTIR and XPS analysis further verified that the hydroxyl groups on the adsorbent were responsible for the sorption of fluoride through the anion exchange and electrostatic interaction in the sorption process. The Mn–Ce hybrid adsorbent has a promising application in the removal of fluoride from aqueous solution in water treatment.

Acknowledgments

We thank the Program for New Century Excellent Talents in University, and the analytical work was supported by the Laboratory Fund of Tsinghua University.

Appendix A. Supplementary data

Supplementary data associated with this article can be found, in the online version, at doi:10.1016/j.jhazmat.2010.12.024.

References

[1] S. Ayoob, A.K. Gupta, Fluoride in drinking water: a review on the status and stress effects, Crit. Rev. Environ. Sci. Technol. 36 (2006) 433–487.
[2] World Health Organization, Guidelines for Drinking-Water Quality: Incorporating First Addendum Recommendations, vol. 1, 3rd ed., World Health Organization, 20 Avenue Appia, 1211 Geneva 27, Switzerland, 2006, pp. 375–376.
[3] A.L. Valdivieso, J.L.R. Bahena, S. Song, R.H. Urbina, Temperature effect on the zeta potential and fluoride adsorption at the α-Al_2O_3/aqueous solution interface, J. Colloid Interface Sci. 298 (2006) 1–5.
[4] N.A. Medellin-Castillo, R. Leyva-Ramos, R. Ocampo-Perez, R.F.G. de la Cruz, A. Aragon-Pina, J.M. Martinez-Rosales, R.M. Guerrero-Coronado, L. Fuentes-Rubio, Adsorption of fluoride from water solution on bone char, Ind. Eng. Chem. Res. 46 (2007) 9205–9212.
[5] L. Lv, J. He, M. Wei, D.G. Evans, Z.L. Zhou, Treatment of high fluoride concentration water by MgAl-CO_3 layered double hydroxides: kinetic and equilibrium studies, Water Res. 41 (2007) 1534–1542.
[6] S. Meenakshi, C.S. Sundaram, R. Sukumar, Enhanced fluoride sorption by mechanochemically activated kaolinites, J. Hazard. Mater. 153 (2008) 164–172.
[7] M. Sarkar, A. Banerjee, P.P. Pramanick, A.R. Sarkar, Use of laterite for the removal of fluoride from contaminated drinking water, J. Colloid Interface Sci. 302 (2006) 432–441.
[8] K. Biswas, D. Bandhoyapadhyay, U.C. Ghosh, Adsorption kinetics of fluoride on iron(III)-zirconium(IV) hybrid oxide, Adsorption 13 (2007) 83–94.
[9] S.P. Kamble, S. Jagtap, N.K. Labhsetwar, D. Thakare, S. Godfrey, S. Devotta, S.S. Rayalu, Defluoridation of drinking water using chitin, chitosan and lanthanum-modified chitosan, Chem. Eng. J. 129 (2007) 173–180.
[10] X.P. Liao, B. Shi, Adsorption of fluoride on zirconium(IV)-impregnated collagen fiber, Environ. Sci. Technol. 39 (2005) 4628–4632.
[11] S. Samatya, U. Yuksel, M. Yuksel, N. Kabay, Removal of fluoride from water by metal ions (Al^{3+}, La^{3+} and ZrO^{2+}) loaded natural zeolite, Sep. Sci. Technol. 42 (2007) 2033–2047.
[12] X.M. Wu, Y. Zhang, X.M. Dou, M. Yang, Fluoride removal performance of a novel Fe–Al–Ce trimetal oxide adsorbent, Chemosphere 69 (2007) 1758–1764.
[13] H. Liu, S.B. Deng, Z.J. Li, J. Huang, G. Yu, Preparation of Al–Ce hybrid adsorbent and its application for defluoridation of drinking water, J. Hazard. Mater. 179 (2010) 424–430.
[14] S.B. Deng, Z.J. Li, J. Huang, G. Yu, Preparation, characterization and application of a nanostructured Ce–Ti adsorbent for enhanced removal of arsenate from water, J. Hazard. Mater. 179 (2010) 1014–1021.
[15] X. Meng, M. Dadachov, G.P. Korfiatis, C. Chritodoulatos, Methods of preparing a surface-activated titanium oxide product and of using same in water treatment processes, 2003, US Patent Application Number 20030155302.
[16] H. Tamura, A. Tanaka, K. Mita, R. Furuichi, Surface hydroxyl site densities on metal oxides as a measure for the ion-exchange capacity, J. Colloid Interface Sci. 209 (1999) 225–231.
[17] Z.J. Li, S.B. Deng, G. Yu, J. Huang, V.C. Lim, As(V) and As(III) removal from water by a Ce–Ti oxide adsorbent: behavior and mechanism, Chem. Eng. J. 161 (2010) 106–113.
[18] H. Chen, H. Chang, Synthesis of nanocrystalline cerium oxide particles by the precipitation method, Ceram. Int. 31 (2005) 795–802.
[19] L. Sicard, J.M. Le Meins, C. Methivier, F. Herbst, S. Ammar, Polyol synthesis and magnetic study of Mn_3O_4 nanocrystals of tunable size, J. Magn. Magn. Mater. 322 (2010) 2634–2640.
[20] H. Chen, A. Sayari, A. Adnot, F. Larachi, Composition–activity effects of Mn–Ce–O composites on phenol catalytic wet oxidation, Appl. Catal., B: Environ. 32 (2001) 195–204.
[21] M.S. Hegde, G. Madras, K.C. Patil, Noble metal ionic catalysts, Acc. Chem. Res. 42 (2009) 704–712.
[22] Y.S. Ho, G. McKay, Pseudo-second-order model for sorption processes, Process Biochem. 34 (1999) 451–465.
[23] G. Lee, C. Chen, S.T. Yang, W.S. Ahn, Enhanced adsorptive removal of fluoride using mesoporous alumina, Microporous Mesoporous Mater. 127 (2010) 152–156.
[24] L. Lv, J. He, M. Wei, D.G. Evans, X. Duan, Factors influencing the removal of fluoride from aqueous solution by calcined Mg-Al-CO_3 layered double hydroxides, J. Hazard. Mater. 133 (2006) 119–128.
[25] S.X. Teng, S.G. Wang, W.X. Gong, X.W. Liu, B.Y. Gao, Removal of fluoride by hydrous manganese oxide-coated alumina: performance and mechanism, J. Hazard. Mater. 168 (2009) 1004–1011.
[26] K. Biswas, S.K. Saha, U.C. Ghosh, Adsorption of fluoride from aqueous solution by a synthetic iron(III)–aluminum(III) mixed oxide, Ind. Eng. Chem. Res. 46 (2007) 5346–5356.
[27] K. Biswas, K. Gupta, A. Goswami, U.C. Ghosh, Fluoride removal efficiency from aqueous solution by synthetic iron(III)-aluminum(III)-chromium(III) ternary mixed oxide, Desalination 255 (2010) 44–51.
[28] X.L. Zhao, J.M. Wang, F.C. Wu, T. Wang, Y.Q. Cai, A.L. Shi, G.B. Jiang, Removal of fluoride from aqueous media by Fe_3O_4@Al$(OH)_3$ magnetic nanoparticles, J. Hazard. Mater. 173 (2010) 102–109.
[29] N.I. Chubar, V.F. Samanidou, V.S. Kouts, G.G. Gallios, V.A. Kanibolotsky, V.V. Strelko, I.Z. Zhuravlev, Adsorption of fluoride, chloride, bromide, and bromate ions on a novel ion exchanger, J. Colloid Interface Sci. 291 (2005) 67–74.
[30] Y. Zhang, M. Yang, X. Dou, H. He, D. Wang, Arsenate adsorption on an Fe-Ce bimetal oxide adsorbent: role of surface properties, Environ. Sci. Technol. 39 (2005) 7246–7253.
[31] E.A. Deliyanni, L. Nalbandian, K.A. Matis, Adsorptive removal of arsenites by a nanocrystalline hybrid surfactant–akaganeite sorbent, J. Colloid Interface Sci. 302 (2006) 458–466.
[32] S.F. Lim, Y.M. Zheng, J.P. Chen, Organic arsenic adsorption onto a magnetic sorbent, Langmuir 25 (2009) 4973–4978.
[33] B.V. Crist, Handbook of Monochromatic XPS Spectra: The Elements and Native Oxides, John Wiley & Sons, LTD, New York, 2000.
[34] M. Machida, M. Uto, D. Kurogi, T. Kijima, MnOx-CeO_2 binary oxides for catalytic NOx sorption at low temperatures, Chem. Mater. 12 (2000) 3158–3164.